Analyst

Redox Cycling-Based Detection of Phenazine Metabolites Secreted from *Pseudomonas aeruginosa* in Nanopore Electrode Arrays

Journal:	*Analyst*
Manuscript ID	AN-ART-10-2020-002022.R1
Article Type:	Paper
Date Submitted by the Author:	14-Dec-2020
Complete List of Authors:	Do, Hyein; University of Notre Dame, Department of Chemistry and Biochemistry Kwon, Seung-Ryong; University of Notre Dame, Department of Chemical and Biomolecular Engineering Baek, Seol; University of Notre Dame, Department of Chemistry and Biochemistry Madukoma, Chinedu; University of Notre Dame, Department of Civil and Environmental Engineering and Earth Sciences Smiley, Marina; Columbia University, Department of Biological Science Dietrich, Lars; Columbia University, Department of Biological Science Shrout, Joshua; University of Notre Dame College of Science, Department of Biological Sciences Bohn, Paul; University of Notre Dame, Department of Chemical and Biomolecular Engineering

Redox Cycling-Based Detection of Phenazine Metabolites Secreted from *Pseudomonas aeruginosa* in Nanopore Electrode Arrays

Hyein Do[1†], Seung-Ryong Kwon[2†], Seol Baek[1], Chinedu S. Madukoma[3,4], Marina K. Smiley[5], Lars E. Dietrich[5], Joshua D. Shrout[3,4,5] and Paul W. Bohn[1,2*]

[1]Department of Chemistry and Biochemistry, University of Notre Dame, Notre Dame, IN, 46556

[2] Department of Chemical and Biomolecular Engineering, University of Notre Dame, Notre Dame, IN, 46556

[3]Department of Civil and Environmental Engineering and Earth Sciences, University of Notre Dame, Notre Dame, IN, 46556

[4]Eck Institute for Global Health, University of Notre Dame, Notre Dame, IN, 46556

[5]Department of Biological Science, Columbia University, New York, 10027

[6]Department of Biological Sciences, University of Notre Dame, Notre Dame, IN, 46556

†Both authors contributed equally to this manuscript.

* Author to whom correspondence should be addressed, pbohn@nd.edu.

Abstract

The opportunistic pathogen *Pseudomonas aeruginosa* (*P. aeruginosa*) produces several redox-active phenazine metabolites, including pyocyanin (PYO) and phenazine-1-carboxamide (PCN), which are electron carrier molecules that also aid in virulence. In particular, PYO is an exclusive metabolite produced by *P. aeruginosa,* which acts as a virulence factor in hospital-acquired infections and is therefore a good biomarker for identifying early stage colonization by this pathogen. Here, we describe the use of nanopore electrode arrays (NEAs) exhibiting metal-insulator-metal ring electrode architectures for enhanced detection of these phenazine metabolites. The size of the nanopores allows phenazine metabolites to freely diffuse into the interior and access the working electrodes, while the bacteria are excluded. Consequently, highly efficient redox cycling reactions in the NEAs can be accessed by free diffusion unhindered by the presence of bacteria. This strategy yields low limits of detection, *i.e.* 10.5 and 20.7 nM for PYO and PCN, respectively, values far below single molecule pore occupancy, *e.g.* at 10.5 nM $\langle n_{pore} \rangle \sim 0.082$ per nanopore - a limit which reflects the extraordinary signal amplification in the NEAs. Furthermore, experiments that compared results from minimal medium and rich medium show that *P. aeruginosa* produces the same types of phenazine metabolites even though growth

rates and phenazine production patterns differ in these two media. The NEA measurement strategy developed here should be useful as a diagnostic for pathogens generally and for understanding metabolism in clinically important microbial communities.

Introduction

The opportunistic pathogen *Pseudomonas aeruginosa* (*P. aeruginosa*) is ubiquitous and is one of the leading causes of hospital-acquired infections. While *P. aeruginosa* rarely grows in healthy individuals, it can cause infections in immunocompromised patients, leading to high rates of mortality and morbidity in patients with cystic fibrosis, burn wounds, and organ transplants.[1-4] Furthermore, the US Centers for Disease Control and Prevention reports that multidrug-resistant *P. aeruginosa* caused 32,600 infections of hospitalized patients and roughly 2,700 deaths in the United States in 2017.[5] Thus, rapid early detection of *P. aeruginosa* is important in order to identify affected patients for treatment in the early stages of infection.

One hallmark characteristic of *P. aeruginosa* is the sequential production of phenazine derivatives starting from chorismic acid: phenazine-1-carboxylic acid (PCA), 5-methylphenazine-1-carboxylic acid (5-MCA), and pyocyanin (PYO) or phenazine-1-carboxamide (PCN), **Figure S1**.[6-8] These phenazines act as virulence factors - generating reactive oxygen species and altering metabolism - that aid the onset of host infection.[9] In particular, PYO is a major virulence factor used by the opportunistic pathogen *P. aeruginosa* in establishing chronic and acute infections. It is involved in suppressing lymphocyte proliferation, interfering with several cellular functions in host cells, and damaging epithelial cells as a consequence of hydroxyl radical formation. Furthermore, PYO has numerous potential effects on various organ systems, *i.e.* respiratory, cardiovascular and central nervous system.[10, 11] Therefore, PYO is a good biomarker, for the bacterial pathogen *P. aeruginosa*,[7, 12] during the early stages of infection.

Various analytical methods, including spectrophotometry, high-performance liquid chromatography, and matrix-assisted-laser-desorption-ionization time-of-flight, have been

explored as a means to identify and monitor *P. aeruginosa* infections.[13-17] Although these methods provide good quantification, extensive sample preparation/treatment steps, such as separation of phenazines from other matrix components, are required, leading to long total analysis times. Alternatively, the redox activity of phenazine derivatives has attracted a great deal of interest as a possible route to a low cost, portable point-of-care device for rapid, early identification of infection. Square wave voltammetry (SWV) and differential pulse voltammetry (DPV) have been used preferentially owing to their sensitivity and good electrochemical resolution in mixtures containing several phenazine derivatives ($E_{1/2}$ = –247 mV, –323 mV and –347 mV *vs*. Ag/AgCl for PYO, PCA and PCN, respectively, at pH 7).[18-21] In addition, different electrode materials and structural configurations have been suggested to improve detection sensitivity further while retaining excellent spatial resolution. For example, integrated circuit-based electrochemical sensors and scanning electrochemical microscopy enable real-time monitoring of phenazine derivatives with high spatial resolution.[19, 22-24] Sensitive electrochemical detection of PYO has thus been achieved using low-cost transparent carbon ultramicroelectrode arrays and paper-based sensors.[12, 25-27]

In the last decade, nanopore electrode arrays (NEAs) have been developed, in which ring-disk dual electrodes separated by an insulating layer (*e.g.* 100 nm silicon nitride) are embedded in each nanopore, creating metal-insulator-metal (MIM) structures in order to exploit enhanced mass transport at the nanoscale. Setting the two electrodes to sufficiently spaced potentials results in rapid, repetitive oxidation and reduction at the two electrodes, *i.e.* redox cycling, producing significantly amplified currents. Strong permselective ion accumulation has also been observed in MIM nanopores, yielding an additional current amplification as large as 2000× with $Ru(NH_3)_6^{3+}$ ($C < 3$ μM) in the absence of supporting electrolyte (SE).[28] Recently, individually

encapsulated NEAs have supported additional current enhancements up to 250-fold beyond those provided by redox-cycling alone, resulting from enhanced mass transport in the nanopores evolving with solution evaporation.[29] Furthermore, adding ion-exchange membranes and block copolymers onto the top surface of NEAs has been used to attain charge-selective current amplification.[30] In addition, NEAs enable the rapid identification of infectious pathogens, because bacterial cells can be directly applied to the surface of NEAs, without the need for further culturing or chemical separations, and the electrochemical scans can be completed in < 30 s. Thus, NEAs are well-suited for early detection and some mitigation against the development of antibiotic resistant strains. All of these results point to the great promise of NEAs for ultrasensitive sensing applications.

Since dual gold electrodes are contained in all nanopores of a typical NEA, the redox cycling current from a single nanopore is multiplied by a factor ~55,000 (*i.e.* total number of pores in 100 × 100 μm^2) yielding a significant current amplification, as shown schematically in **Figure 1(a)-(b)**. In addition, comparing the size of a planktonic *P. aeruginosa* cell with the diameter of nanopores (*i.e.* ~300 nm at the pore opening), makes it clear that the much larger bacteria - and their accompanying excreted extracellular polymeric substances - are excluded from the interior of the nanopores, making the NEAs resistant to biofouling over the time course of these experiments, while allowing the small phenazine metabolites to diffuse into the nanopores to participate in redox cycling reactions, **Figure 1(c)-(d)**. Here, we demonstrate the highly sensitive electrochemical detection of phenazine metabolites in NEAs, which can be used for rapid detection of *P. aeruginosa*. Highly sensitive detection of phenazine derivatives is achieved in the NEAs using redox cycling-based cyclic-voltammetry (CV). SWV, a complementary technique, is also used to characterize and distinguish the redox activity of the

phenazine metabolites. The dynamics and concentration profiles of phenazine production have previously been reported for two nutritionally rich growth media: Lysogeny broth (LB) and tryptic soy broth (TSB).[12] In the present study, we compare phenazine production for *P. aeruginosa* grown in rich (LB) and defined minimal nutrient medium as a function of time. Although the same phenazine metabolites are produced in these conditions, different bacterial growth rates and patterns of phenazine production are observed, which is attributed to the different nutrient conditions in FAB and LB media. The redox cycling-based highly sensitive detection of phenazine production developed in this study can be useful for early diagnostics of bacterial infections as well as the development of sensitive biosensors for other pathogens.

Experimental Section

Chemicals and Materials. Pyocyanin and phenazine-1-carboxamide were purchased from Sigma-Aldrich (St. Louis, MO), and phenazine-1-carboxylic acid was purchased from SynQuest Laboratories (Alachua, FL). Difco Lysogeny Broth (LB), Lennox, purchased from BD Biosciences (Sparks, MD), and modified Fastidious Anaerobe Broth (FAB) were used to grow *P. aeruginosa* strains.[31]

Bacterial Loading in NEA Devices. NEAs were fabricated according to previously reported procedures from this laboratory.[29, 30, 32, 33] In order to confirm that the nanopores excluded bacteria, a bacteria-loaded NEA device was prepared and analyzed using scanning electron microscopy (SEM, FEI-Helios dual-beam focused ion beam). To prepare the samples, 80 μL of *P. aeruginosa* LB culture at OD 2.51 was transferred onto the top surface of an NEA. Then, after waiting 10 min for the bacteria to settle, the NEA device was gently washed with LB medium and DI water and then dried. SEM images were taken to analyze the *P. aeruginosa*-

loaded NEA at an accelerating voltage of 5 kV and an electron beam current of 0.1 nA. All samples were coated with 5 nm Ir prior to SEM imaging to prevent surface charging.

Preparation of Phenazine Standards. For the phenazine calibration curves, stock solutions (1 mM PYO, 200 μM PCA, and 200 μM PCN) were first prepared for each phenazine in FAB medium augmented with 30 mM glucose. The phenazine stock solutions were then serially diluted to 10 nM, 50 nM, 100 nM, 1 μM, 10 μM, and 100 μM in FAB medium and used directly for electrochemical measurements.

Bacterial Strains and Cell Culture Preparation. P. aeruginosa PA14 wild-type (*wt*),[34] Δ*phz*MS (which produces PCN and PCA, but not PYO),[19] and Δ*phz* (phenazine-null),[35] strains were used in this study. Bacteria strains were streaked from frozen (-80 °C) stock onto LB plates (1.5% agar w/v) and incubated overnight at 37 °C. Isolated colonies were transferred to test tubes containing either 6 mL FAB minimal medium supplemented with 30 mM glucose,[34, 36] or LB medium with 30 mM glucose, and incubated at 37 °C on a shaker table at 240 rpm. Optical density at 600 nm [OD_{600}] of these samples was determined every 2 h or 1 h for FAB- and LB-grown cultures, respectively, using an Eppendorf BioPhotometer Plus, after which 500 μL of the culture was collected at each time point and preserved at 4 °C.

Electrochemical Measurements. In order to perform electrochemical measurements, *ca*. 100 μL of *P. aeruginosa* LB or FAB culture at various OD values was transferred to a poly(dimethylsiloxane) (PDMS) well mounted to the NEA device. Square wave voltammetry (SWV) and cyclic voltammetry (CV) were performed using a CHI842C electrochemical workstation (CH Instruments, USA). For SWV and non-generator-collector (non-GC) mode CV, the bottom gold disk electrode (*i.e.* BE) was used as working electrode in a three-electrode system with external Pt wire counter and Ag/AgCl reference electrodes. For GC mode operation,

both disk (BE) and ring (*i.e.* TE) gold electrodes were used as working electrodes in a four-electrode system. All cyclic voltammograms were obtained with a scan rate of 0.1 V s^{-1}. SWV was performed using a potential increment of 4 mV and a potential amplitude of 25 mV at a frequency of 15 Hz. NEA devices were reusable. The process of transferring the cultured cells to the NEA surface and acquiring the electrochemical measurement typically took 2-3 min for both CV and SWV.

Results and Discussion

Fabrication and Electrochemical Function of NEAs. High density NEAs (~5.5 pores μm^{-2}) with ~350 nm pore-to-pore center distance were produced over a 100 μm × 100 μm area based on a combination of reactive-ion etching and nanosphere lithography, as shown schematically in **Figure 1(a)**. Each individual nanopore (V_{pore} ~ 13 aL) contains a 150 nm diameter Au bottom disk electrode separated by a 100 nm SiN_x dielectric layer from the 100 nm thick top Au ring electrode, as shown schematically in **Figure 1(b)**. Thus, electro-active redox species in the nanopores are able to undergo rapid redox cycling reactions at the top and bottom Au electrodes (TE and BE, hereafter), resulting in a significant current amplification.[28-30, 32, 33] Furthermore, because the bacteria are applied directly to the NEA surface, secreted factors need only diffuse a few μm, at most, to reach the electrochemically active volume, thereby greatly reducing the response time of the sensor. The 100 nm hydrophilic silicon dioxide (SiO_2) layer was deposited as the topmost layer to protect the TE and to facilitate nanopore filling with aqueous electrolyte and/or secreted factors from *P. aeruginosa*.

Cyclic voltammetry (CV) was performed using 5 mM $Fe(CN)_6^{3/4-}$ in 2 M KNO_3 to demonstrate the redox cycling-based current amplification. An excess concentration of

supporting electrolyte (SE), *i.e.* 2 M KNO_3, was used to minimize ion migration, so that a diffusion-limited current response was obtained. At first, the non-generator-collector (non-GC) mode response, *i.e.* no redox cycling, was measured using either BE or TE as working electrode in a 3-electrode system with Ag/AgCl reference and Pt wire counter electrodes while leaving the other nanopore-confined working electrode at open-circuit potential. As shown in **Figure 2(a)**, TE and BE produced similar non-GC mode currents, with the current at TE being somewhat larger due to its closer proximity to bulk solution. Both BE and TE were then employed as working electrodes in a 4-electrode system to achieve generator-collector (GC) mode operation, with redox cycling between TE and BE. **Figure 2(b)** shows 35-fold current amplification in GC mode compared to non-GC mode current obtained at BE. The symmetric cathodic and anodic currents at BE and TE in GC mode indicate ~100% collection efficiency, in which the molecules reduced at BE are efficiently collected and re-oxidized at TE and *vice versa*. Enhanced current (16-fold) was also observed in GC mode with PYO, a phenazine metabolite, **Figure 2(c)**.

Electrochemistry of Phenazines in Biological Growth Media. The voltammetric responses of PYO were measured in FAB growth medium in both non-GC and GC modes. **Figure S2** displays the voltammograms of 100 μM PYO obtained by (*a*) scanning the potential of BE (E_{BE}) between +0.2 V and –0.8 V while TE was at open circuit (*i.e.* non-GC mode), (*b*) scanning E_{BE} between -0.8 V and +0.2 V while holding E_{TE} = –0.8 V (*i.e.* GC mode), or (*c*) scanning E_{BE} between +0.2 V and -0.8 V while holding E_{TE} = +0.2 V (*i.e.* GC mode in the opposite sense). As expected, GC mode operation exhibits a current enhancement in either sense.

However, when working electrode potentials more negative than –0.4 V were applied, a noticeable background current was observed and superimposed on the faradaic current of PYO in both GC mode (at BE, dashed line in red and at TE, solid line in blue) and non-GC mode, as

shown in **Figure S2**. Consequently, the cathodic background (*vide infra*) contributes to the asymmetry between the two GC mode currents in **Figure S2**. This cathodic background makes up a larger proportion of the total current with decreasing analyte (PYO) concentration. In this regard, GC mode operation provides another benefit, in addition to current amplification, since the cathodic background current can be avoided by choosing the anodic current. Hereafter, anodic currents are displayed and used in case of the GC mode operation for the detection and monitoring of phenazine derivatives.

Next, calibration curves for PYO, PCN, and PCA were generated using both redox cycling-enabled CV and SWV. The GC mode anodic currents allowed highly sensitive detection for all three phenazines. The limits of detection (LOD) based on 3σ/slope[37] were determined to be 10.5 nM, 20.7 nM, and 52.2 nM for PYO, PCN, and PCA respectively, as shown in **Figures 3(a)** and **(b)** and **Figure S3** (also see **Figures S4(a)**, **S5(a)**, and **S6(a)** for representative anodic GC currents). As shown in **Figure S3** and **Figure S6(a)**, the higher LOD for PCA also corresponds to lower currents at high concentration, *e.g.* i_{lim} = 142, 57, and 6.8 nA for PYO, PCN, and PCA, respectively, at 100 μM), which may result from the low solubility of PCA in aqueous solution.[38, 39] Furthermore, the currents increase monotonically over the entire range 10 nM - 100 μM, with PYO exhibiting good linearity over the entire range, while PCA and PCN are linear from 10 nM - 10 μM and slightly superlinear above 10 μM. Thus, the NEAs not only produce low LODs, but also substantial dynamic range, covering the biologically relevant 1-100 μM range. In some cases, especially after exposure to high concentration (≥ 100 μM) solutions, a residual due to polymerized phenazines was observed. These residuals were readily removed by repeating several CV scans consecutively, thereby recovering a clean electrode surface.

For PYO at the 10.5 nM LOD, the number of molecules occupied in the entire nanopore

array (~5.5×10^4 pores) is estimated to be ~ 4520 molecules (~7.5 zmoles), corresponding to $\langle n_{pore} \rangle \sim 0.0822$. Accessing and measuring samples of this limited extent clearly marks the advantage of redox cycling current amplification using NEAs. SWV of PYO and PCN, however, produced very different results than GC mode CV measurements. Whereas **Figure S4(a)** clearly shows that PYO produces a detectable CV signal at 10 nM, the SWV shows a strong background feature at *ca.* -0.42 V, presumably arising from electroactive components of the FAB medium. As shown in **Figure S4(b)** and **S4(c)**, addition of PYO results in a shift and decrease in the magnitude of this peak, but it is not until a concentration of 10 μM is reached that a clear PYO SWV peak can be identified. Then at 100 μM, the PYO peak dominates the background (**Figures S4(b,c)** *inset*). Similar behavior was observed for PCN, as shown in **Figure S5**. In addition, PCA was obscured by the SWV background over the entire concentration range from 10 nM to 100 μM, **Figure S6**. The background likely arises from competitive electrochemical reactions involving molecular oxygen, glucose, and other species including minor components of the complex FAB medium. Independent of the source of the background, **Figures S4(b)-(c)**, **S5(b)-(c)**, and **S6(b)-(c)** all clearly show that the SWV background current dominates the analyte signal at concentrations ≤ 10 μM for PYO, PCN, and PCA. The important conclusion from these experiments is that, compared to other electroanalytical methods reported for the detection of phenazines and to the SWV results reported here, the redox cycling-based electrochemical detection using NEAs exhibits substantially lower LOD values.[40] It is noteworthy that, as shown in **Figure S7**, PYO generates the highest current response at 100 μM among the three phenazines, an observation that we tentatively assign to analyte-dependent electrochemical kinetics for the proton-coupled electron transfer reaction.

Although GC mode-enabled redox cycling produces significant current enhancement and

can distinguish PYO from PCN and PCA due to the different onset potentials, *ca*. –0.3 V for PYO and *ca.* –0.4 V for PCA and PCN in **Figure S7(a)**, it is rather difficult to distinguish PCN and PCA due to their overlapping responses in the GC mode voltammograms. In this context, SWV is beneficial as a complementary tool in identifying phenazine species and improving chemical resolution in mixtures.[12, 19, 27, 41] Unlike the GC mode voltammograms, oxidative and reductive SW voltammograms of the phenazines show peak current responses at different potentials with reasonable chemical resolution, as shown in **Figure S7(b)-(c)**. Hence, combining information from both GC mode CV and SWV in NEAs affords highly sensitive detection of the phenazine metabolites as well as good chemical resolution.

Monitoring of Phenazine Metabolites Produced by P. aeruginosa. We previously used a combination of electrochemistry and surface-enhanced Raman spectroscopy to investigate the redox behavior of PYO from *P. aeruginosa* and to map 2D PYO distributions as a function of pH and electrochemical potential on a roughened gold surface.[36] Here, we extend those studies using NEAs, in order to take advantage of the sensitivity resolution demonstrated above. *P. aeruginosa* was grown under two different sets of conditions - using a minimal nutrient medium, and nutrient-rich LB medium, which is capable of supporting a more robust metabolic level - and the production of phenazine metabolites was followed for either 10 h or 28 h culturing times. Culture samples were collected at various OD values (times) and transferred onto the outer surface of the NEAs, after which GC mode CV and SWV were performed to monitor the production of phenazine metabolites (see **Table S1** for the correlation of collection times with OD values).

With no bacteria present, control experiments employing GC mode CV generated the lowest currents, consistent with lack of secreted phenazines, **Figure 4(a)**. Starting at samples with OD $\geq$ 1.66 GC mode CVs show increasing currents with increasing OD values. Two broad

waves are observed, at −0.45 V and −0.7 V, corresponding to the potentials expected for PYO and PCN/PCA, respectively, indicating that multiple phenazine species are produced by *P. aeruginosa* in sufficient quantities to be detected by NEA-based GC mode CV experiments. Consistent with the GC mode CV data, the SWV voltammograms obtained from samples at OD ≥ 1.66 also show shoulders at more negative potentials, **Figure 4(b)** and **Figure S8**. Interestingly, small continuous negative shifts in peak potential were observed which are attributed to slight pH changes upon cell growth, *e.g.* ΔpH ~ +0.06 from the initial point upon adding cells to fresh LB medium to an OD of 2.51 after incubation. Furthermore, by comparing the current values measured from NEAs under both GC mode CV and SWV conditions, it is possible to estimate the concentration of PYO detected from the PA14 *wt* samples grown to OD 1.66 in LB medium to be ~1.5 μM. Therefore, the NEA-based analytical platform not only enables highly sensitive detection of phenazine metabolites, but it enables semi-quantitative estimates of metabolite secretion levels. Since PYO is the final product in the biosynthetic route (**Figure S1**), it accumulates with increasing incubation time and thus, dominates the other two phenazines at longer times as more of the precursors are converted to the PYO end-product. The blue-green color of *P. aeruginosa* PA14 grown in LB medium, **Figure S9**, also supports the predominance of PYO production. It is also noteworthy that, as indicated earlier, anodic GC mode voltammograms show only background response after cleaning with several CV scans, even if the NEA device was previously used for *P. aeruginosa* grown to high OD values in LB medium, as shown in **Figure S10**.

While PYO was predominant over the other phenazines after long incubation times, smaller features were observed at other potentials. For example, a single broad peak at *ca*. −0.56 V was observed in the SWV voltammograms of lower-OD samples, **Figure 4(b)**. Additional

experiments with the *P.aeruginosa* Δ*phzMS* mutant strain, which produces only PCA and PCN, show a single current wave at *ca.* –0.50 V, **Figure S11**. Additional small current waves were observed at *ca*. –0.14 V and 0.02 V with increasing incubation time, **Figure 4(b)**. Previous studies have identified 5-MCA, another phenazine metabolite in the PYO pathway, as being responsible for these features in the PA14 *wt* strain.[12, 19, 42]

P. aeruginosa grown in minimal medium produced SWV features at the same positions as phenazine metabolites (–0.44 V for PYO, –0.57 V for PCA, PCN, and –0.08 V and 0.12 V for 5-MCA), but showed different bacterial growth rate and production pattern of phenazine metabolites compared to growth in nutrient-rich LB medium, **Figure 5**. For example, as expected, *P. aeruginosa* (PA14 *wt*) cultured in LB yielded higher OD values than cultures grown in minimal medium at 10 h, OD = 2.50 (LB) and OD = 0.315 (FAB) owing to their different growth rates, **Table S1**. Interestingly, SWV voltammograms exhibit a stronger background response in FAB than in LB medium, *cf.* **Figure 5(b)** and **Figure S12**, but even the presence of a small amount of secreted phenazines, *e.g.* OD = 0.118, is sufficient to suppress the background. Because LB and FAB media consist of different mixtures of chemical and biological components, different background current levels are expected in different media. Nonetheless, the lowest background current in the GC mode voltammogram in **Figure 5(a)** confirms no phenazine production in FAB medium in the absence of *P. aeruginosa*, so that the background current response in the SWV voltammograms does not result from phenazine species. In addition, **Figure S13** shows the GC mode CV and SWV responses from a FAB-grown Δ*phz* mutant, which produces no phenazine metabolites. The SWV background peak at -0.6 V in **Figure 5(b)** is clearly missing, suggesting that while background suppression occurs when phenazines are secreted, the phenazine metabolites themselves may not be responsible. Instead, background

suppression could plausibly be the result of a co-secreted compound that itself is not electrochemically active in this potential window.

In comparing *P. aeruginosa* PA14 grown on LB and minimal media, both conditions lead to predominant production of PYO but exhibit different phenazine production patterns. While measurable amounts of PCN, PCA and 5-MCA were detected in addition to PYO from growth in minimal medium, only marginal amounts of those phenazines were detected in LB medium. Thus, the time course of phenazine production is altered quantitatively, taking much longer to reach the same production levels on minimal medium compared to nutrient-rich LB.

Conclusion

In this study, dual-electrode-embedded nanopore arrays are used for highly sensitive electrochemical detection and real-time monitoring of phenazine metabolites produced by *P. aeruginosa*. Owing to the size exclusion character of nanopore arrays (~300 nm at the pore opening), the phenazine metabolites can diffuse into the nanopores and undergo rapid redox cycling reactions at the dual electrodes, while the larger bacteria and associated EPS are excluded from the interior of the nanopore arrays, thus realizing significant current amplification without interference from the bacterial cells themselves. GC-mode-enabled redox cycling CV and SWV are used in a complementary fashion in the NEAs in order to achieve highly sensitive detection as well as good chemical resolution for identifying phenazines electrochemically. GC mode CV successfully detected phenazine metabolites with high sensitivities, showing LODs of 10.5 nM and 20.7 nM for PYO and PCN, respectively. Compared to other reported values, GC mode CV produces substantially lower LODs, demonstrating the advantage of NEAs to achieve signal amplification.[40]

NEAs were also used to monitor phenazine production from *P. aeruginosa* grown in nutrient-rich and minimal media. In both media, the same phenazine species are produced, but show different bacterial growth rates and phenazine production patterns. While PYO is dominantly detected under both media conditions, PCA and PCN are detected with PYO in minimal medium, but produce only small current responses in LB medium, demonstrating different phenazine production patterns with time. Another minor phenazine species, 5-MCA was also detected in both growth media. The difference in the dynamics of phenazine production under the two growth conditions suggests that nutrients contribute to the variance in phenazine production rates and concentrations.[8] Electrochemical sensing using NEAs is thus a promising new approach for monitoring bacterial secreted metabolites with enhanced sensitivity, and the approach has the potential to significantly improve the early detection of infectious pathogens in point-of-care diagnostics.

Acknowledgements

This work was supported by National Science Foundation grant NSF1904196 (development and characterization of NEAs for phenazine detection) and the Office of Science of the US Department of Energy grant DE-SC0019312 (characterization of *P. aeruginosa* phenazine secretion). Structures were constructed at the Notre Dame Nanofabrication Facility, and the authors express their appreciation to the staff for their expert assistance and guidance. L.E.D. was supported by NIH/NIAID grant no. R01 AI103369.

References

1. C. W. M. Bedrossian, S. Donald Greenberg, D. B. Singer, J. J. Hansen and H. S. Rosenberg, *Hum. Pathol.*, 1976, **7**, 195-204.
2. T. S. Walker, H. P. Bais, E. Déziel, H. P. Schweizer, L. G. Rahme, R. Fall and J. M. Vivanco, *Plant Physiol.*, 2004, **134**, 320-331.
3. B. Tümmler and C. Kiewitz, *Mol. Med. Today*, 1999, **5**, 351-358.
4. R. B. Fick, Jr., *Chest*, 1989, **96**, 158-164.
5. Centers for Disease Control and Prevention (CDC), Antibiotic Resistance Threats in the United States, http://dx.doi.org/10.15620/cdc:82532, Atlanta, GA, 2019.
6. M. Mentel, E. G. Ahuja, D. V. Mavrodi, R. Breinbauer, L. S. Thomashow and W. Blankenfeldt, *ChemBioChem*, 2009, **10**, 2295-2304.
7. D. V. Mavrodi, T. L. Peever, O. V. Mavrodi, J. A. Parejko, J. M. Raaijmakers, P. Lemanceau, S. Mazurier, L. Heide, W. Blankenfeldt, D. M. Weller and L. S. Thomashow, *Appl. Environ. Microbiol.*, 2010, **76**, 866-879.
8. M. Z. El-Fouly, A. M. Sharaf, A. A. M. Shahin, H. A. El-Bialy and A. M. A. Omara, *J. Radiat. Res. Appl. Sci.*, 2015, **8**, 36-48.
9. S. Hall, C. McDermott, S. Anoopkumar-Dukie, A. J. McFarland, A. Forbes, A. V. Perkins, A. K. Davey, R. Chess-Williams, M. J. Kiefel, D. Arora and G. D. Grant, *Toxins*, 2016, **8**, 236.
10. P. Nadal Jimenez, G. Koch, J. A. Thompson, K. B. Xavier, R. H. Cool and W. J. Quax, *Microbiol. Mol. Biol. Rev.*, 2012, **76**, 46-65.
11. B. Rada and T. L. Leto, *Trends Microbiol.*, 2013, **21**, 73-81.

12. O. Simoska, M. Sans, M. D. Fitzpatrick, C. M. Crittenden, L. S. Eberlin, J. B. Shear and K. J. Stevenson, *ACS Sens.*, 2019, **4**, 170-179.

13. F. Y. Al-Ani, A. S. Al-Shibib, K. M. Khammas and R. Taher, *Fol. Microbiol.*, 1986, **31**, 215-219.

14. A. Croxatto, G. Prod'hom and G. Greub, *FEMS Microbiol. Rev.*, 2012, **36**, 380-407.

15. D. V. Mavrodi, R. F. Bonsall, S. M. Delaney, M. J. Soule, G. Phillips and L. S. Thomashow, *J. Bacteriol.*, 2001, **183**, 6454-6465.

16. J. H. K. Chen, P.-L. Ho, G. S. W. Kwan, K. K. K. She, G. K. H. Siu, V. C. C. Cheng, K.-Y. Yuen and W.-C. Yam, *J. Clin. Microbiol.*, 2013, **51**, 1733-1739.

17. R. Wilson, D. A. Sykes, D. Watson, A. Rutman, G. W. Taylor and P. J. Cole, *Infect. Immun.*, 1988, **56**, 2515-2517.

18. Y. Wang and D. K. Newman, *Environ. Sci. Technol.*, 2008, **42**, 2380-2386.

19. D. L. Bellin, H. Sakhtah, J. K. Rosenstein, P. M. Levine, J. Thimot, K. Emmett, L. E. P. Dietrich and K. L. Shepard, *Nat. Commun.*, 2014, **5**, 3256.

20. T. Seviour, L. E. Doyle, S. J. L. Lauw, J. Hinks, S. A. Rice, V. J. Nesatyy, R. D. Webster, S. Kjelleberg and E. Marsili, *Chem. Commun.*, 2015, **51**, 3789-3792.

21. A. Buzid, F. Shang, F. J. Reen, E. Ó. Muimhneacháin, S. L. Clarke, L. Zhou, J. H. T. Luong, F. O'Gara, G. P. McGlacken and J. D. Glennon, *Sci. Rep.*, 2016, **6**, 30001.

22. D. L. Bellin, H. Sakhtah, Y. Zhang, A. Price-Whelan, L. E. P. Dietrich and K. L. Shepard, *Nat. Commun.*, 2016, **7**, 10535.

23. D. Koley, M. M. Ramsey, A. J. Bard and M. Whiteley, *Proc. Natl. Acad. Sci. USA*, 2011, **108**, 19996-20001.

24. J. L. Connell, J. Kim, J. B. Shear, A. J. Bard and M. Whiteley, *Proc. Natl. Acad. Sci. USA*, 2014, **111**, 18255-18260.

25. F. A. a. Alatraktchi, J. S. Noori, G. P. Tanev, J. Mortensen, M. Dimaki, H. K. Johansen, J. Madsen, S. Molin and W. E. Svendsen, *PLoS One*, 2018, **13**, e0194157.

26. O. Simoska, M. Sans, L. S. Eberlin, J. B. Shear and K. J. Stevenson, *Biosens. Bioelectron.*, 2019, **142**, 111538.

27. J. Elliott, O. Simoska, S. Karasik, J. B. Shear and K. J. Stevenson, *Anal. Chem.*, 2017, **89**, 6285-6289.

28. C. Ma, N. M. Contento and P. W. Bohn, *J. Am. Chem. Soc.*, 2014, **136**, 7225-7228.

29. S.-R. Kwon, K. Fu, D. Han and P. W. Bohn, *ACS Nano*, 2018, **12**, 12923-12931.

30. K. Fu, D. Han, S.-R. Kwon and P. W. Bohn, *ACS Nano*, 2018, **12**, 9177-9185.

31. A. Heydorn, A. T. Nielsen, M. Hentzer, C. Sternberg, M. Givskov, B. K. Ersbøll and S. Molin, *Microbiology*, 2000, **146**, 2395-2407.

32. C. Ma, N. M. Contento, L. R. Gibson and P. W. Bohn, *ACS Nano*, 2013, **7**, 5483-5490.

33. K. Fu, D. Han, C. Ma and P. W. Bohn, *Faraday Discuss.*, 2016, **193**, 51-64.

34. J. D. Shrout, D. L. Chopp, C. L. Just, M. Hentzer, M. Givskov and M. R. Parsek, *Mol. Microbiol.*, 2006, **62**, 1264-1277.

35. L. E. P. Dietrich, A. Price-Whelan, A. Petersen, M. Whiteley and D. K. Newman, *Mol. Microbiol.*, 2006, **61**, 1308-1321.

36. H. Do, S.-R. Kwon, K. Fu, N. Morales-Soto, J. D. Shrout and P. W. Bohn, *Langmuir*, 2019, **35**, 7043-7049.

37. J. Mocak, A. M. Bond, S. Mitchell and G. Scollary, *Pure Appl. Chem.*, 1997, **69**, 297-328.

38. Z.-J. Yang, H.-B. Hu, X.-H. Zhang and Y.-Q. Xu, *J. Chem. Eng. Data*, 2007, **52**, 184-185.

39. J. C. Hill and G. T. Johnson, *Mycologia*, 1969, **61**, 452-467.

40. O. Simoska and K. J. Stevenson, *Analyst*, 2019, **144**, 6461-6478.

41. T. A. Webster, H. J. Sismaet, J. L. Conte, I. J. Chan and E. D. Goluch, *Biosens. Bioelectron.*, 2014, **60**, 265-270.

42. C. R. Santiveri, H. J. Sismaet, M. Kimani and E. D. Goluch, *ChemistrySelect*, 2018, **3**, 2926-2930.

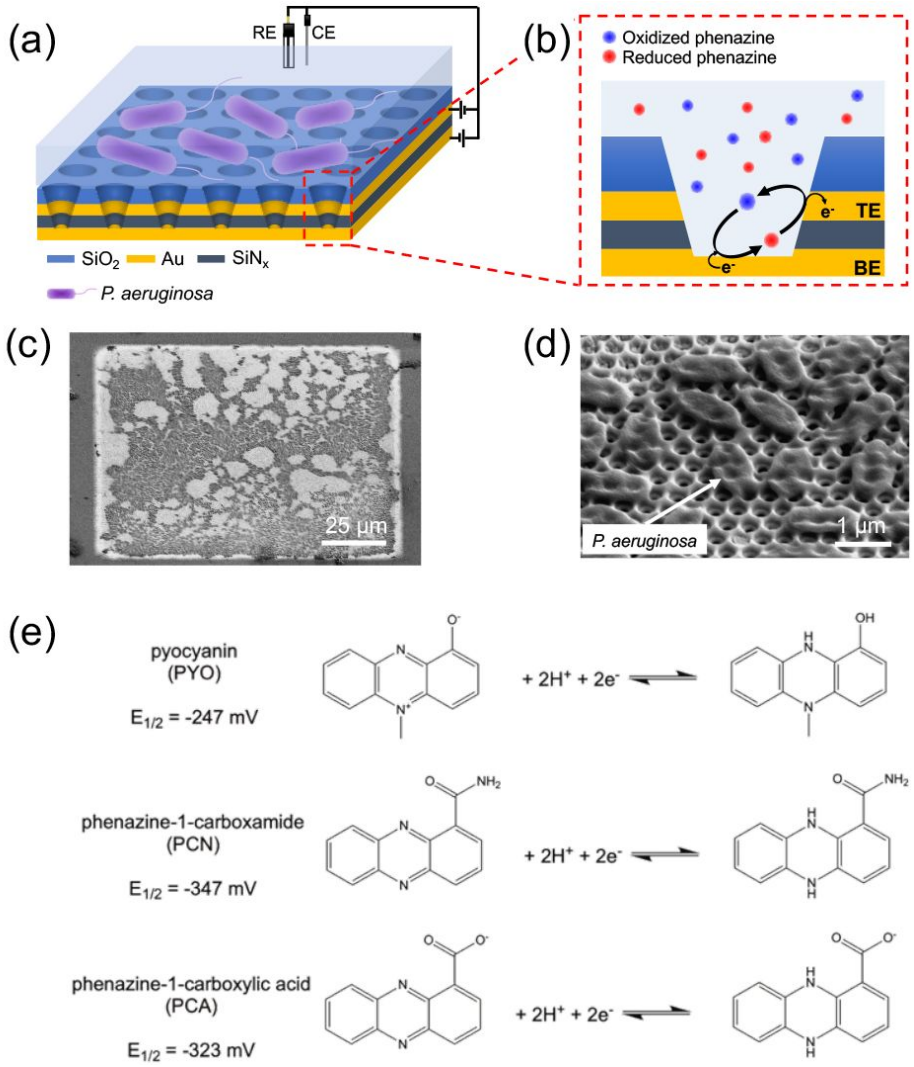

Figure 1. (a) Schematic illustration showing the dual gold electrode-embedded NEA device loaded with *P. aeruginosa* in a growth medium. (b) Schematic diagram illustrating redox cycling-based current amplification of phenazine metabolites in the NEA while bacteria remain outside of the nanopore due to size-exclusion. (c,d) SEM images of a *P. aeruginosa*-loaded NEA tilted at 52 degrees showing the whole NEA (c) and an enlarged area (d). The bright rectangular area is the whole NEA and the gray spots indicate bacterial clusters residing at the outer NEA surface. (e) Electrochemical reaction schemes of phenazine metabolites with redox potentials relative to Ag/AgCl at pH 7.

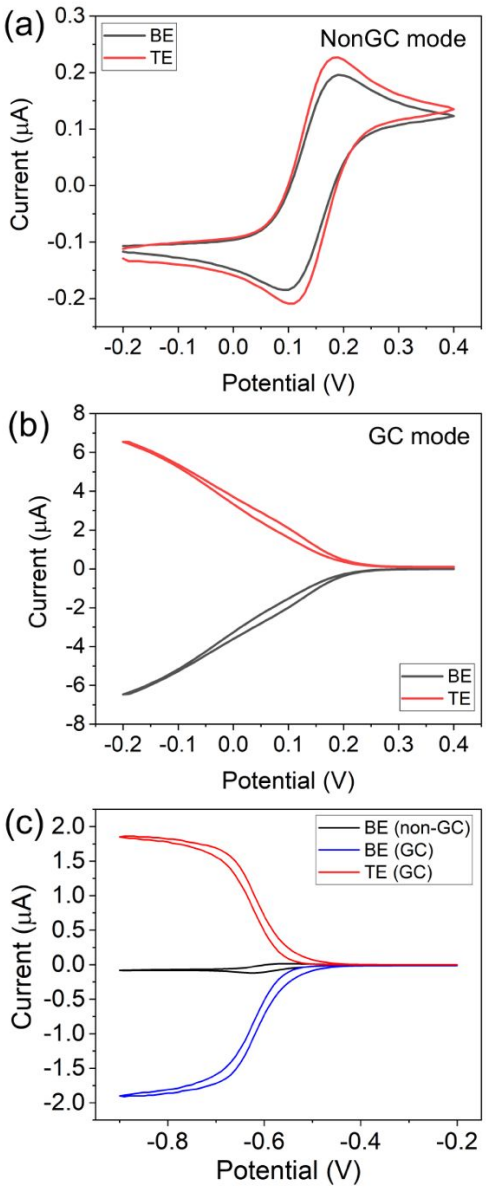

Figure 2. Voltammograms of (a,b) 5 mM $Fe(CN)_6^{3/4-}$ in 2 M KNO_3 and (c) 1 mM PYO in 2 M KNO_3. Non-GC voltammograms (a and c in black) obtained in a 3-electrode system, with either BE or TE as working electrode with a Pt wire counter and a Ag/AgCl reference electrode. In GC mode operation (b and c in red and blue), BE was scanned negative while TE was held at E_{TE} = 0.4 V (b) or –0.2 V (c) *vs*. Ag/AgCl to achieve redox cycling in a 4-electrode configuration. All voltammograms were obtained at a scan rate of 0.1 V s^{-1}.

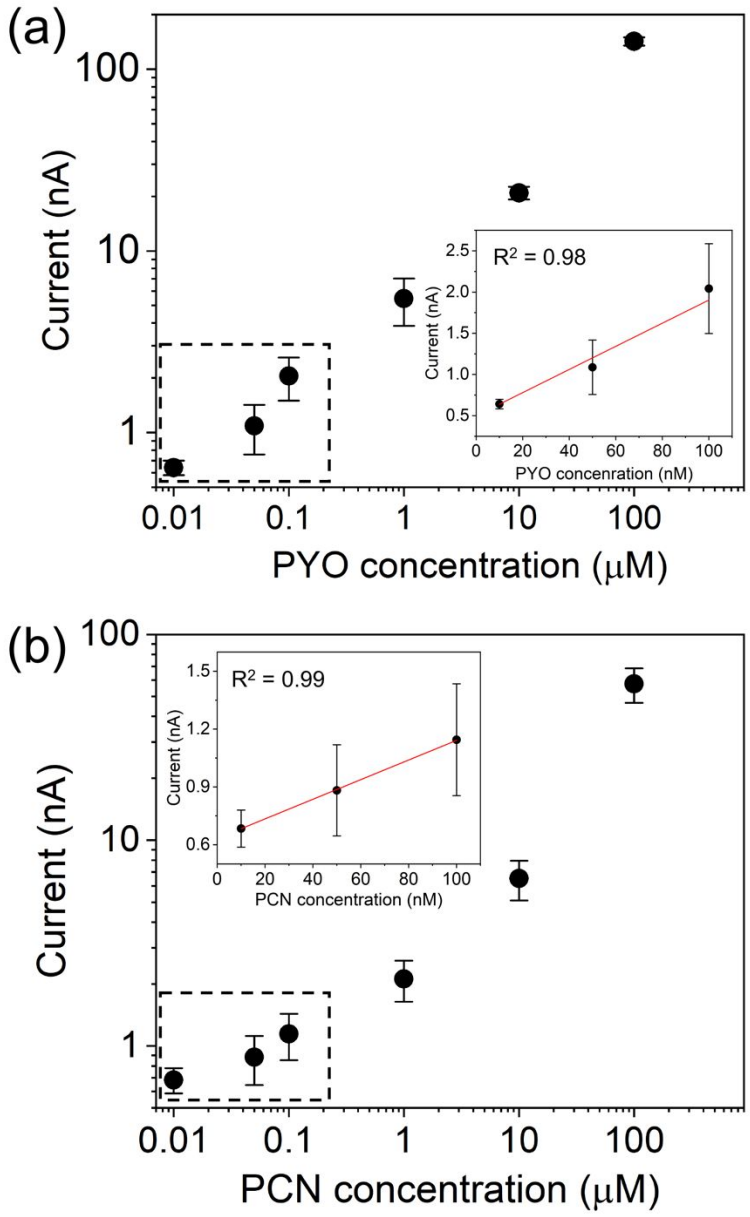

Figure 3. Calibration plots for (a) PYO and (b) PCN generated from the GC mode voltammograms. The anodic current at E_{TE} = +0.2 V was taken for the calibration curves when E_{BE} was at –0.8 V during its potential sweep. (*Insets*) Current responses in the concentration range from 10 to 100 nM. The mean values and error bars (standard deviation) were obtained from three independent measurements.

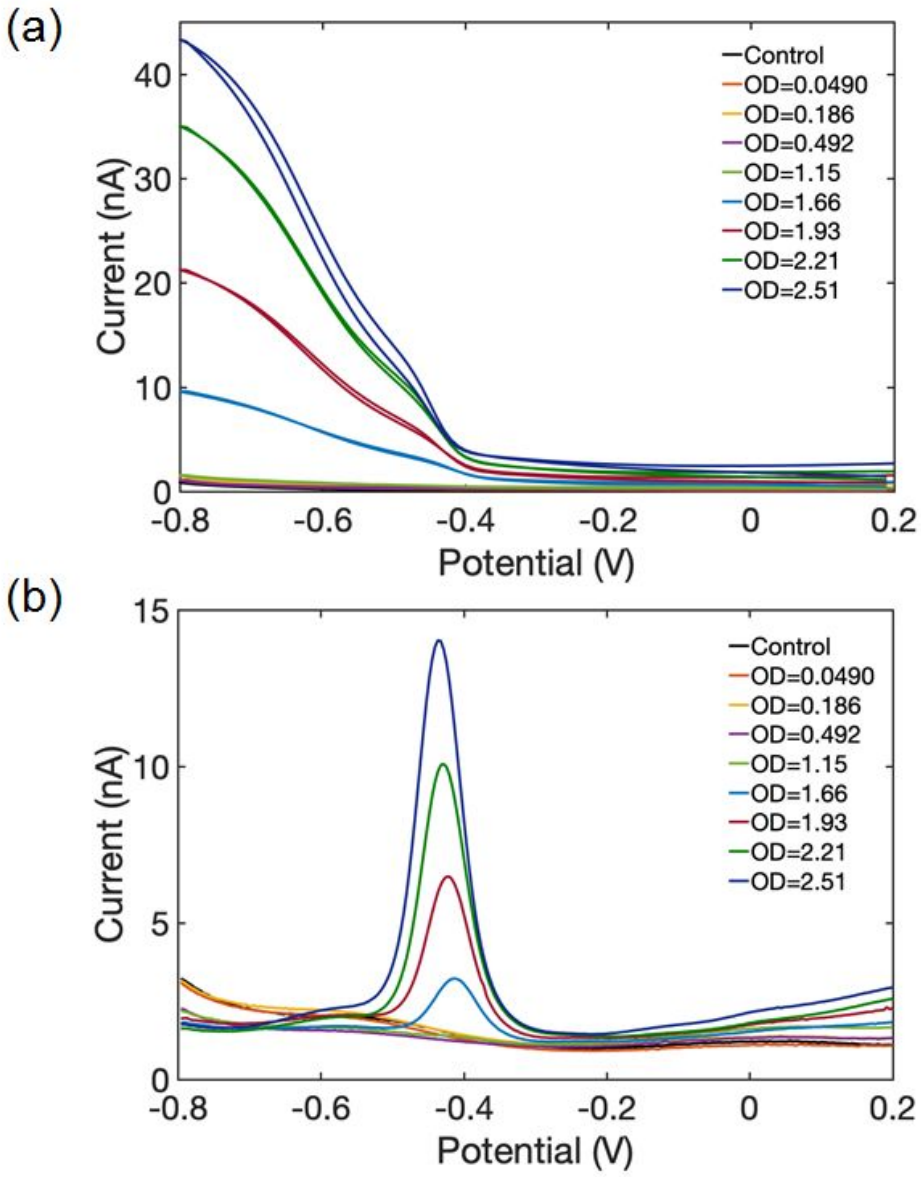

Figure 4. (a) GC mode cyclic-voltammograms and (b) oxidative SW voltammograms obtained after adding *P. aeruginosa* (PA14 *wt*) grown in nutrient-rich LB medium to the indicated OD values (increasing growth time) on NEAs. OD values above 0.8 should be considered approximate due to multiple scattering effects. Cyclic voltammograms were obtained at a scan rate of 0.1 V s^{-1}, and potential was scanned starting at +0.2 V.

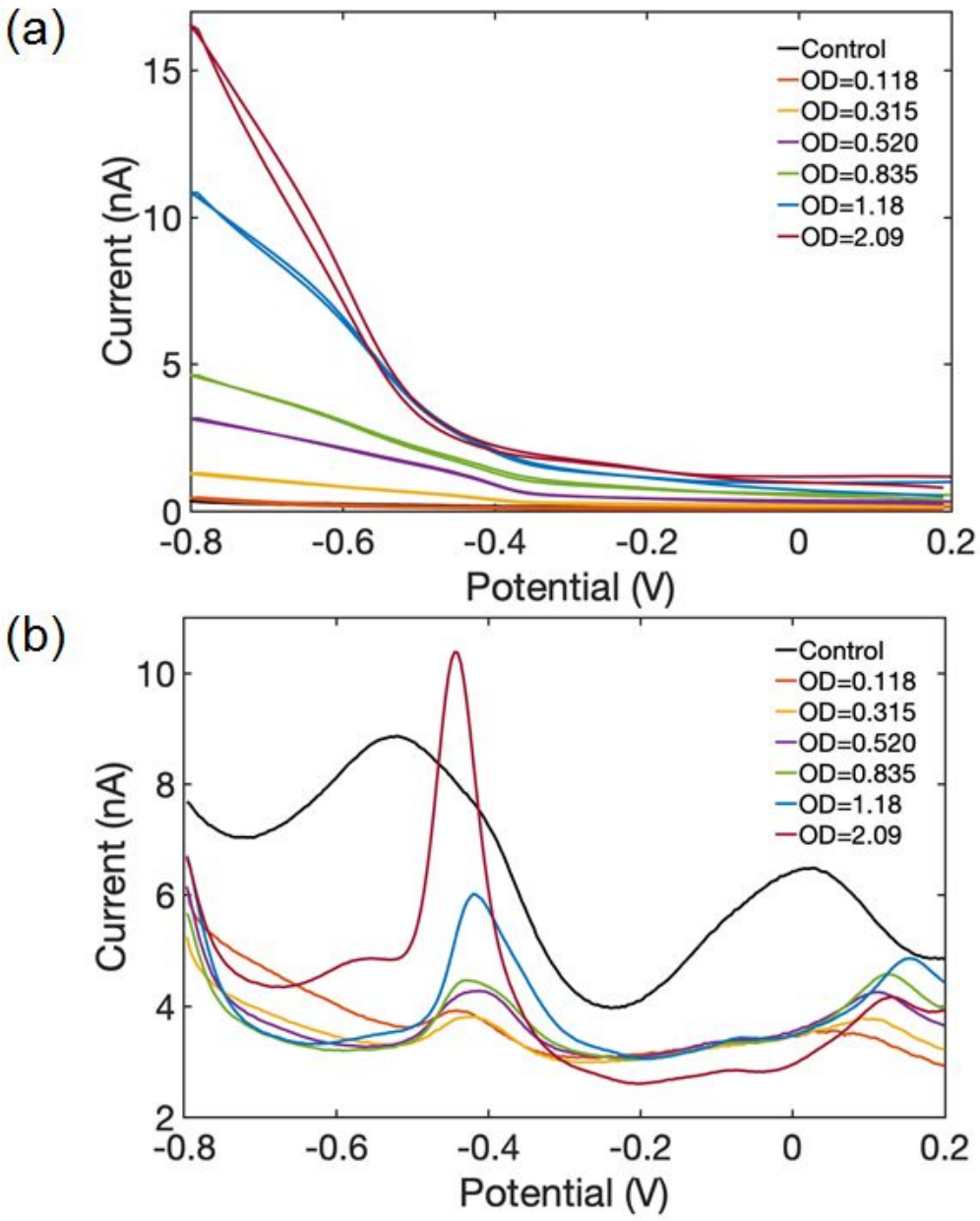

Figure 5. (a) Anodic GC mode cyclic-voltammograms and (b) oxidative SW voltammograms obtained in *P. aeruginosa* (PA14 *wt*) grown in FAB minimal medium to increasing OD values (increasing growth time). OD values above 0.8 should be considered approximate due to multiple scattering effects. Cyclic voltammograms were obtained at a scan rate of 0.1 V s^{-1}, and potential was scanned starting at +0.2 V.